Biomedicine & Pharmacotherapy 151 (2022) 113214

Contents lists available at ScienceDirect

Biomedicine & Pharmacotherapy

journal homepage: www.elsevier.com/locate/biopha

Cytotoxic effect of metformin on butyrate-resistant PMF-K014 colorectal cancer spheroid cells

Kesara Nittayaboon [a], Kittinun Leetanaporn [a], Surasak Sangkhathat [a], Sittirak Roytrakul [b], Raphatphorn Navakanitworakul [a,*]

[a] Department of Biomedical Sciences and Biomedical Engineering, Faculty of Medicine, Prince of Songkla University, Hat Yai, Songkhla 90110, Thailand
[b] National Center for Genetic Engineering and Biotechnology (BIOTEC), National Science and Technology Development Agency, Pathumthani 12120, Thailand

ARTICLE INFO

Keywords:
Colorectal cancer cell
Butyrate resistance
Metformin
Spheroid cell

ABSTRACT

Three-dimensional (3D) cell culture models are used in cancer research because they mimic physiological responses in vivo compared with two-dimensional (2D) culture systems. Recently, cross-resistance of butyrate-resistant (BR) cells and chemoresistance in colorectal cancer (CRC) cells have been reported; however, effective treatments for BR cells have not been identified. In this study, we investigated the cytotoxicity of metformin (MET), an anti-diabetic drug, on BR CRC cells in a 3D spheroid culture model. The results demonstrate that MET decreases spheroid size, migration, and spheroid viability, while it increases spheroid death. The molecular mechanism revealed that AMP-activated protein kinase (AMPK) and Akt serine/threonine kinase 1(Akt) were significantly upregulated, whereas the acetyl-CoA-carboxylase (ACC) and mammalian target of rapamycin (mTOR) were downregulated, which led to caspase activation and apoptosis. Our findings show the potential cytotoxicity of MET on CRC-BR cells. The combination of MET and conventional chemotherapeutic drugs should be addressed in further studies to reduce the side effects of standard chemotherapy for CRC.

1. Introduction

Based on the GLOBOCAN 2020 data, colorectal cancer (CRC) is the third most commonly diagnosed cancer and the second cause of cancer-related death in both men and women worldwide [1]. In Thailand, CRC is the third most common cancer. The incidence and mortality are increasing despite the existence of more effective screening programs and treatments [2,3]. Previous reports have demonstrated that butyrate, a bacterial metabolite present in the human colon, contributes to chronic inflammation and CRC development [4,5]. Butyrate normally inhibits the proliferation of cancer cells and induces apoptosis; however, long-term exposure can alter cancer cells to generate butyrate-resistant (BR) cells. BR cells exhibit various malignant phenotypes, including glucose deprivation survival, heat-shock tolerance, and increased tumorigenicity [6,7]. Previous reports have suggested that BR cells contribute to the chemoresistant phenotype, causing the treatments to fail[8]. Moreover, an AMP-activated protein kinase (AMPK)-activating compound exerted effects on BR cells, including proliferation inhibition and autophagy activation [9]. These AMPK activator drugs appear to sensitize BR cells.

Metformin (MET) is commonly used to treat diabetes mellitus (DM) but, surprisingly, it was also shown to reduce the risk of cervical, endometrial, lung, and colon cancers in type 2 DM patients [10–13]. MET acts by inhibiting mitochondrial respiration, resulting in an imbalance in the AMP:ATP ratio, which is regulated by AMPK [14,15]. Previous studies have shown that MET, which activates AMPK, is a candidate therapeutic agent against chemoresistant CRC cells when combined with 5-fluorouracil (5-FU) and oxaliplatin (Ox, FuOx) [13]. Moreover, a study of breast cancer cell lines revealed that MET pre-treatment reduces the doxorubicin-resistant phenotype [16]. Based on these findings, MET may exhibit therapeutic effects against drug-resistant cancer cells.

Three-dimensional (3D) spheroid culture is widely used in cancer research. Compared with two-dimensional (2D) or monolayer cultures, the 3D culture model can mimic the tumor environment in vivo [17,18]. Various reports have suggested that 3D CRC-primary cells could preserve the characteristic of their parental tumor tissue [19] and show a different response during irradiation and chemotherapy [20]. Previous

* Corresponding author.
E-mail addresses: kesara.nittayaboon@gmail.com (K. Nittayaboon), lkittinun1@gmail.com (K. Leetanaporn), s.sangkhathat@gmail.com (S. Sangkhathat), sittiruk@biotec.or.th (S. Roytrakul), nraphatp@medicine.psu.ac.th (R. Navakanitworakul).

https://doi.org/10.1016/j.biopha.2022.113214
Received 27 February 2022; Received in revised form 24 May 2022; Accepted 26 May 2022
Available online 28 May 2022

studies conducted using a 3D breast cancer model revealed a different phenotype, including hypoxia in the bulk tumor and drug sensitivity, which was higher compared with that observed in the 2D system [21]. The 3D CRC cells also showed a reduction of cancer drug activity [22]. Moreover, the effects of drugs in a 3D cell culture model of BR cells have not been thoroughly investigated.

In this study, we characterized the formation of PMF-k014 cells-derived spheroids and determined the cytotoxic effect of MET on PMF-k014 BR spheroids. The drug response was evaluated in terms of cell viability, caspase3/7 activity, and spheroid migration. The underlying molecular mechanism was examined by Western blot analysis.

2. Materials and methods

2.1. Butyrate-resistant cell culture

PMF-k014 epithelial colorectal carcinoma——a polygonal epithelial derived from highly metastatic adenocarcinoma [23] (RBRC-RCB1426, RIKEN BRC, Japan)——cells were grown in Dulbecco's modified Eagle's medium (Gibco™ Thermo Fisher, USA) supplemented with 10 % heat-inactivated fetal bovine serum (Gibco™ Thermo Fisher scientific, USA) and 1 % penicillin/streptomycin (Gibco™ Thermo Fisher scientific, USA) in a humidified incubator with 5 % CO_2 and 95 % air at 37 °C. The butyrate-resistant PMF (PMF-BR) cells were previously established (unpublished data). Briefly, the cells were stimulated in a complete medium supplemented with 0.2 mM sodium butyrate (Sigma, USA). Butyrate treatments induced cancer cell death. However, some cells survived and continued to proliferate. BR cells were subcultured at 80 % confluency. Subsequently, the concentration of butyrate was increased by 2-fold every three generations. After the concentration of butyrate reached 3.2 mM, both the parental (PT) and BR cells were ready for further experiments.

2.2. Poly-HEMA-coated plate preparation and spheroid formation

A stock solution of poly-(2-hydroxyethyl methacrylate) (Poly-HEMA, Sigma, USA) was prepared at 120 mg/mL in 95 % ethanol by stirring with a sterile magnetic bar at room temperature overnight. A working solution was prepared (5 mg/mL) using the same procedure. Then, 20 μL of working solution was added to a 96-well U-bottom plate, and the plate was dried for 3 days in an incubator. The spheroids were generated by seeding PMF-PT and PMF-BR cells in the coated plate to generate 200–300 μm spheroid cells.

2.3. Characterization of spheroid formation

To detect the presence of CD44 surface marker, immunofluorescence assay was used. We fixed the spheroids in 4 % paraformaldehyde for 20 min. Then, fixed spheroids were incubated with antihuman CD44 (phycoerythrin [PE] conjugated; ImmunoTools, Germany) for 45 min. The nuclei were counterstained with 4′,6-Diamidine-2′-phenylindole dihydrochloride (DAPI) (Sigma, USA). The stained spheroids were imaged on a LionheartFX live cell imager (Biotek, USA).

To assess the genes expression, total RNA was isolated from the monolayer and spheroid cells using the Trizol reagent (Invitrogen, USA) as instructed by the manufacturer. RNA was then quantified using absorbance measurements by Nanodrop (Thermo Fisher). RNA samples (1 μg) with good quality were reverse-transcribed to complementary DNA (cDNA) using reverse transcriptase enzymes. An iScript™ cDNA synthesis kit (Bio-rad, USA) was used for cDNA synthesis according to the manufacturer's instructions. *GAPDH* was used as an internal control. Differential expression of stemness genes; *SOX2*, *OCT4*, *KLF4* and *CXCR4*, butyrate-related genes; *GPR-109A*, *GPR-109B, GPR-41* and *SLC5A8* and drug efflux genes; *ABCA5*, *ABCC1*, *ABCC2*, *ABCC3*, *ABCC5*, *ABCF2* and *ABCG2* were determined. The primer sequences are shown in Supplementary Table 1. The quantitative real time RT-PCR (RT-qPCR) was carried out in duplicates with three independent experiments. The $2^{-\Delta Ct}$ method was used for calculating the relative gene expression levels.

2.4. Characterization of PMF-PT and PMF-BR spheroids by mass spectrometry

To examine the characteristics of PMF-PT and PMF-BR spheroids, mass spectrometry was performed at the Functional Proteomics Technology Laboratory, National Center for Genetic Engineering and Biotechnology (BIOTEC), Thailand. The spheroid cell lysates were reduced, alkylated, and digested with trypsin, and were analyzed by LC-MS/MS (Bruker Impact II, USA). Peptides were quantified and identified using the DeCyder MS differential analysis software 2.0 (GE Healthcare, USA) and the MASCOT search engine (Matrix Science, UK) based on the NCBI human protein databases. To display the list comparing PT and BR spheroids, the peptide data were used to generate Venn diagrams through jvenn, an interactive Venn diagram viewer (http://jvenn.toulouse.inra.fr/app/index.html). The functional enrichment analysis of the uniquely expressed proteins was performed using the PANTHER analysis tool (http://pantherdb.org/).

2.5. Butyrate sensitivity

Both the monolayer cells and spheroids generated on poly-HEMA-coated plates were treated with and without butyrate (Sigma, USA) at various concentrations (0–100 mM) for 72 h. After incubation, cell viability was measured using ApoLive-Glo™ Multiplex Assay (Promega, USA) following the manufacturer's instructions. Briefly, the fluorescent substrate (glycyl-phenylalanyl-amino fluorocoumarin; GF-AFC) was added to the treated spheroids. Live-cell protease was interacted with GF-AFC substrate. The fluorescent intensity was detected following a 400 nm excitation source and 505 nm emission filter, was then quantified using a Varioskan LUX multimode microplate reader (Thermo Fisher, USA), and was presented as the percentage of cell viability.

2.6. MET activity in butyrate-resistant spheroids

The spheroids generated on poly-HEMA coated plates were treated with and without MET at various concentrations for 72 h. After incubation, spheroid size, cell viability, and caspase activity were measured. The spheroid size was firstly determined using an inverted microscope and was analyzed using ImageJ analysis software. The LIVE/DEAD® Cell Imaging Kit (Thermo Fisher scientific, USA) was used for staining. The solution contained calcein AM and BOBO-3 iodide, which interacted with live and dead cells, respectively. The complete media of spheroids were removed until 100 μL was left in each well. Then, the mixed solution was added, and the plate was wrapped with aluminum foil to protect the contents from sunlight, and it was further incubated at 37 °C for 30 min. The images were obtained using a LionheartFX live cell imager. The ApoLive-Glo™ Multiplex Assay was used to detect viable cells as a marker of cytotoxicity, and caspase3/7 activation as a marker of apoptosis. The kit contains two assay components. Firstly, the activity of a protease marker of cell viability was measured. The protease activity of live cells was restricted to intact viable cells and was measured using a fluorogenic and cell-permeant peptide substrate (GF-AFC). The substrate entered intact cells where it was cleaved by the protease activity of live cells to generate a fluorescent signal proportional to the number of living cells, which was measured as relative fluorescence units using the following 400 nm excitation source and 505 nm emission filter. The protease of live cells is inactive as the cell membrane integrity is lost and leakage occurs into the culture medium. Secondly, the kit also contained the Caspase-Glo® assay which is used to detect caspase 3/7 activation. This assay provides a luminogenic caspase-3/7 substrate, which contains the tetrapeptide sequence DEVD, in a reagent optimized for caspase activity, luciferase activity, and cell lysis. Adding the Caspase-Glo®

3/7 reagent resulted in cell lysis, followed by caspase cleavage of the substrate and generation of a luminescent signal produced by luciferase. Luminescence is proportional to the amount of caspase activity present and was measured as relative luminescence units using the Caspase-Glo 3/7 assay system. Both assays were quantified with a Varioskan LUX multimode microplate reader. The means of three independent experiments were plotted as a dose response curve.

2.7. Spheroid migration

The migration properties of PMF-PT and PMF-BR spheroids were evaluated using a tumor spheroid-based migration assay. Briefly, PMF-PT and PMF-BR spheroids were generated by seeding the cells into 96-well U-bottom Poly-HEMA coated plates for 72 h, and were further incubated with MET at various concentrations for 72 h. Then, the spheroids were transferred to a new flat-bottom 96-well plate and further incubated for 72 h. After incubation, the spheroids were imaged using an inverted microscope (10x magnification). The migration areas were analyzed using ImageJ software.

2.8. Western blot analysis

Western blot analysis with spheroids was performed as previously described [24]. Briefly, spheroid pellets were lysed in RIPA buffer (Pierce Biotechnology, USA). Protein concentration was measured using the Bradford assay (Bio-Rad, USA). Protein extract with 30 μg was subjected to SDS-polyacrylamide gel electrophoresis (SDS-PAGE) followed by transfer to polyvinylidene difluoride (PVDF) membranes (Amersham Pharmacia Biotech, USA). The membranes were blocked in 5 % non-fat milk in Tris-buffer saline with 0.1 % (v/v) Tween-20 (TBS-T) for 1 h at room temperature. Then, they were washed twice with TBS-T for 10 min. Each membrane was incubated overnight at 4 °C, shaking continuously with primary antibodies (1:1000 diluted with 1 % non-fat milk in TBS-T) specific to AMPKα (cat. no. 5831; Cell Signaling Technology, Inc.), phospho-AMPKα (Thr172, cat. no. 2535; Cell Signaling Technology, Inc.), acetyl-CoA carboxylase (cat. no. 3676; Cell Signaling Technology, Inc.), phospho-acetyl-CoA carboxylase (Ser79; cat. no. 11818; Cell Signaling Technology, Inc.), Akt (cat. no. 4691; Cell Signaling Technology, Inc.), phospho-Akt (Ser473; cat. no. 4060; Cell Signaling Technology, Inc.), phospho-mTOR (Ser2448; cat. no. 5536; Cell Signaling Technology, Inc.), mTOR (cat. no. 2983; Cell Signaling Technology, Inc.), Raptor (cat. no. 2280; Cell Signaling Technology, Inc.), Rictor (cat. no. 2114; Cell Signaling Technology, Inc.), GβL (cat. no. 3274; Cell Signaling Technology, Inc.) and β-actin (cat. no. 4967; Cell Signaling Technology, Inc.) used as internal control. After incubation, the membranes were washed thrice (10 min/time) with TBS-T and were incubated with a secondary antibody (Anti-rabbit IgG horseradish peroxidase; cat. no. 7074; Cell Signaling Technology, Inc.) at 1:1000 diluted in 1 % non-fat milk in TBS-T for 2 h. Then, the membranes were washed again three times with TBS-T and the last washing was performed using TBS for 10 min. The protein expressions were visualized using an enhanced chemiluminescence reagent (Pierce™ ECL Western Blotting Substrate, Thermo Fisher scientific, USA). Densitometry was performed using a Chemiluminescence & Epi Fluorescence Alliance Q9 Advanced (Uvitec, UK) imager.

3. Results

3.1. PMF-PT and PMF-BR spheroid formation and characterization

We first evaluated the butyrate sensitivity on the butyrate-induced monolayer cells that were incubated with or without various concentrations of butyrate and determined the 50 % inhibitory concentration (IC_{50}). We found that the IC_{50} value of PMF-BR cells was 3-fold higher than that of PMF-PT cells. Moreover, both PT and BR cells were treated with various concentrations of anticancer drugs such as 5-FU and MET for 72 h. We found that butyrate-resistant cells were cross-resistant to 5-FU, whereas both PT and BR cells were sensitive to MET with an equal IC_{50} value of MET (Supplementary Table 1).

Currently, several promising drug candidates tested using the 2D culture model have not proved successful in clinical practice. Therefore, we focused on the 3D culture model. PMF-PT and PMF-BR cells were grown on poly-HEMA-coated plates for 72 h to generate spheroids. Both cells formed spheroids with a round-shape structure, compact morphology, and smooth surface. The size of PMF-PT spheroids was slightly larger than that of PMF-BR spheroids (Fig. 1A). The average diameter of the PT spheroid was 208.29 ± 7.94 μm, whereas that of the BR spheroid was 196.41 ± 9.43 μm. We also characterized spheroid formation by detection of the presence of CD44 as cancer stem cell (CSC) marker on the surface of spheroids using immunofluorescence staining. CD44 was positively stained in the membrane of cells in spheroids in both spheroids (Fig. 1A). In addition, we investigated CSC enrichment in formed spheroids as compared to their 2D monolayers. The expression of key stemness genes including *SOX2*, *OCT4*, *KLF4* and *CXCR4* using RT-qPCR were assessed. We found that the expression of *SOX2* and *OCT4* genes were significantly upregulated in both PMF-PT and BR spheroids as compared to their 2D monolayers, while the expression of *KLF4* and *CXCR4* was not difference in both comparisons (Fig. 1B-C).

For butyrate sensitivity tests, both spheroids were incubated with various concentrations of butyrate, and IC_{50} was then determined. The viability of PMF-BR spheroids was significantly higher than that of PMF-PT spheroids. The percentage of cell survival and the IC_{50} of each spheroid cell are shown in Fig. 2A and B, respectively. The IC_{50} value of PMF-BR spheroids was 2.7 times higher than that of PMF-PT spheroids. This result indicated that the BR spheroid still presents the trait of butyrate resistance. We also examined the response of the spheroids against 5-FU, which is normally used in clinical practice (Supplementary Figure 1). The IC_{50} values of 5-FU in PMF-PT and PMF-BR spheroids were 78.50 ± 5.95 and 208.80 ± 4.77 μM, respectively. This result illustrated that the PMF-BR spheroids were also cross-resistant to 5-FU. Moreover, the expression of butyrate-related genes and drug efflux pumps was determined using *GAPDH* as an internal control. *GPR109A*-a butyrate receptor-its homolog *GPR109B*, *GPR-41* and sodium-couplet monocarboxylate transporter 1 (*SMCT1* or *SLC5A8*) are response to the transport of bacterial metabolites-particularly butyrate-in intestinal cells. PMF-BR spheroids showed significantly higher expression of *GPR-109A*, *GPR-109B* and *GPR-41* genes than that of PMF-PT spheroids, whereas *SLC5A8* was not difference in both spheroids (Fig. 2C). For evaluating the expression of the efflux pump, the expression of the ABC-binding cassette transporter genes, which plays an important role in drug transport in cancer cells, was elucidated. PMF-BR spheroids showed significantly higher expression of *ABC-C1*, *ABC-C2*, *ABC-C3*, *ABC-C5* and *ABC-G2* genes than PMF-PT spheroids. The expression of *ABC-A5* was significantly low in PMF-BR spheroids, whereas *ABC-F2* was not difference in both spheroids (Fig. 2D).

The protein expression profiles in both spheroid cell types were also identified by LC-MS/MS and then compared and visualized using a Venn's diagram (Fig. 2E). This demonstrated all the possible relations of protein expressions and the uniquely expressed proteins found in PMF-PT and PMF-BR spheroids. The names of the uniquely expressed proteins found only in PMF-PT and in PMF-BR spheroid cells are listed in Supplementary Table 3 and Supplementary Table 4, respectively. These uniquely expressed proteins were subsequently subjected to functional enrichment analysis using PANTHER based on their pathway. We found that the unique proteins involved in the metabolic pathway and signal reception and transduction were enriched in PMF-BR spheroids rather than in PMF-PT spheroids. In addition, proteins related to apoptosis and stress response, transcriptional and posttranscriptional process, cell cycle control and proliferation, and DNA replication and repair were enriched only in PMF-BR spheroids. However, the unique proteins involved in the cytoskeleton structure and cell–matrix interactions were found in only PMF-PT spheroids (Fig. 2F).

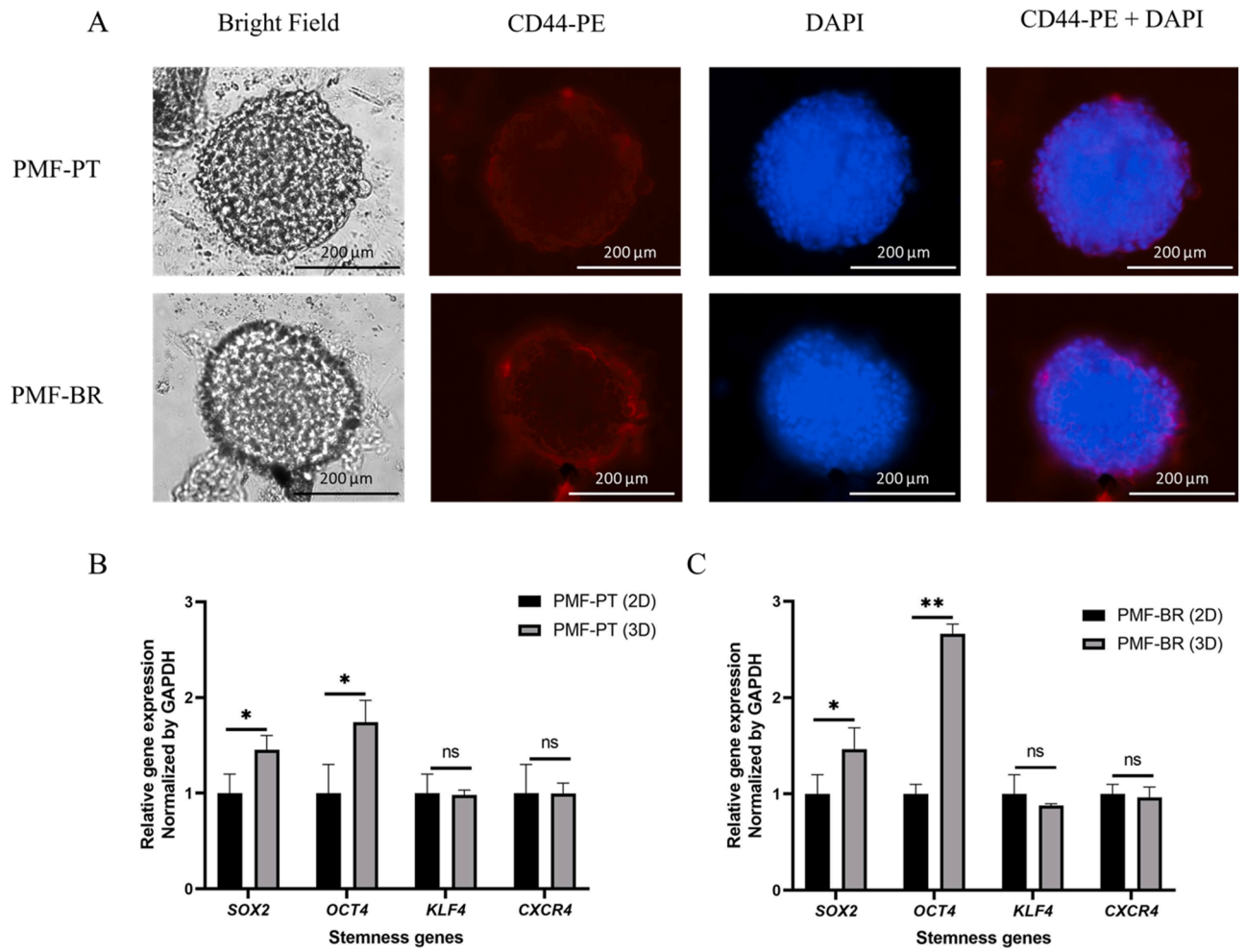

Fig. 1. Morphology of PMF-PT and PMF-BR spheroids and their characteristics. Spheroids were formed by seeding the cells on poly-HEMA coated plates for 72 h and stained with CD44-PE (red) and DAPI (blue). Their images were obtained using an inverted microscope with 10x magnification (scale bar = 100 µm) (A). Relative expression of stemness genes in PMF-PT (B) and PMF-BR (C) was performed using RT-qPCR. Gene expression levels are shown relative to those of GAPDH. Data are shown as mean ± standard deviation (SD) of triplicate experiments (* *p-value* < 0.05 and ** *p-value* < 0.01; the mean difference is significant at the 0.05 and 0.01 level, respectively compared between 2D and 3D via Student's *t*-test. Abbreviations: PMF-PT, PMF parental cells; PMF-BR, butyrate-resistant PMF cells; DAPI, 4′,6-Diamidine-2′-phenylindole dihydrochloride.

3.2. MET effect on PMF-PT and PMF-BR spheroids

3.2.1. MET reduces the size of PMF-PT and PMF-BR spheroids

The spheroid size was determined upon treatment (Day 0) and after 72 h (Day 3). Spheroid diameter was measured using ImageJ analysis software. Briefly, the scale bar was calibrated in a micrometer unit. Then, the spheroid diameter was measured by a linear line across the edge. The software then converted the pixels of the linear line into micrometer. Fig. 3 shows decreasing spheroid size in a dose-dependent manner. However, spheroid size increased at 100 mM, possibly due to cell death and disaggregation.

3.2.2. MET induces PMF-PT and PMF-BR spheroid death

After 72 h of treatment with MET, the viability of the spheroids was determined using the LIVE/DEAD staining kit. The kit distinguishes live and dead cells using two probes, namely calcein AM for intracellular esterase activity and BOBO-3 iodide for plasma membrane integrity. The results indicated that MET-induced spheroid death as evidenced by a red fluorescent signal in the treatment group, whereas viable cells showed a green fluorescent signal in the control (Fig. 4).

3.2.3. MET reduces cell viability and induces caspase activity in PMF-PT and PMF-BR spheroids

To investigate the mode of cell death, we used the ApoLive-Glo assay to measure enzyme activity as a marker for viable cells, and caspase-3/7 activity as an indication of apoptosis. We found that MET decreased cell viability and increased caspase-3/7 activity in the treatment group (Fig. 5). The caspase-3/7 activity of PMF-BR spheroids at all concentrations was higher than that of PMF-PT, even though the percentage of cell viability was equal in both spheroid cell types. These results suggested that PMF-BR spheroids are sensitive to MET, resulting in apoptosis.

3.2.4. MET reduces spheroid migration in PMF-PT and PMF-BR cells

The anti-migration of MET on PT and BR spheroids was evaluated using a tumor spheroid-based migration assay [25]. After MET treatment for 72 h, the spheroids were transferred to a new flat-bottom plate containing fresh complete media and were further incubated for 72 h. Then, the migration area of the spheroids was measured and calculated as the percentage of spheroid migration. The results showed a significant decrease in migration at 25- and 50-mM MET for PMF-PT and at 50 mM for PMF-BR spheroids (Fig. 6). This indicated that MET may have anti-migration properties in both spheroid cell types, with even significant effects on PMF-PT spheroids.

A

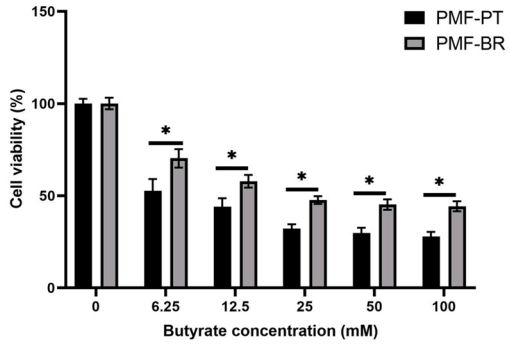

B

Cell lines	Butyrate (mM, mean ± SD)	Fold
PMF-PT	8.17 ± 0.67	2.7
PMF-BR	22.09 ± 0.12	

C

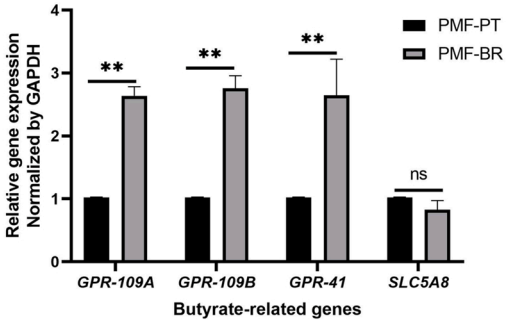

D

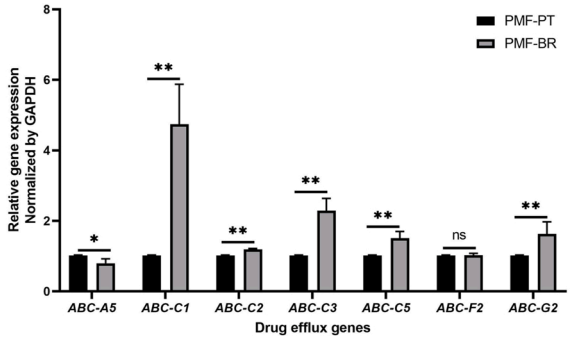

E

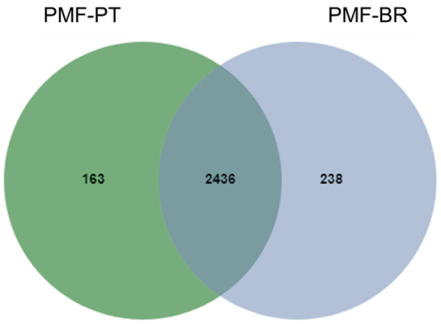

F

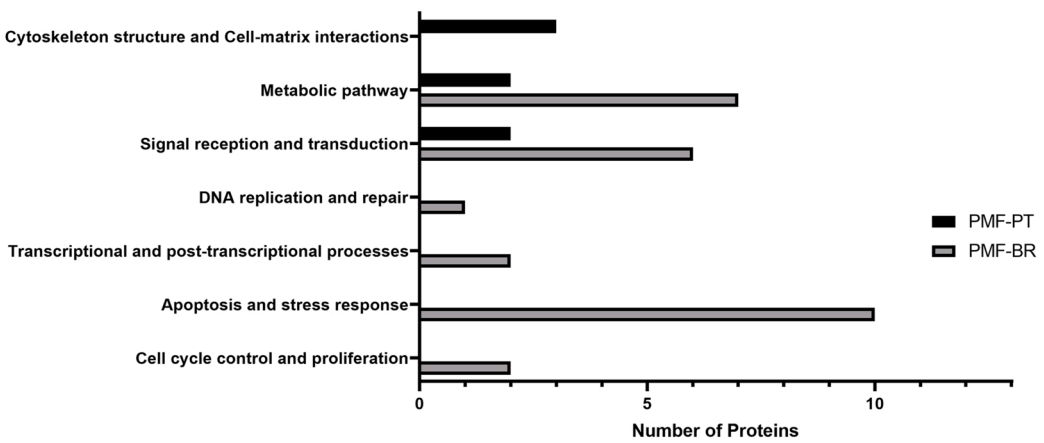

Fig. 2. Characterization of butyrate resistance spheroids. Effect of butyrate on PMF-PT and PMF-BR spheroids for 72 h represented as percentage of cell viability (A). The IC_{50} value of butyrate after the 72-h treatment was estimated from dose response curves (B). Relative expression of butyrate-related genes (B) and drug efflux genes (C) in the spheroids was perform using RT-qPCR. Gene expression levels are shown relative to those of GAPDH. Data are shown as mean ± standard deviation (SD) of triplicate experiments (* *p-value* < 0.05 and ** *p-value* < 0.01; the mean difference is significant at the 0.05 and 0.01 level compared between PMF-PT and PMF-BR spheroids via Student's *t*-test. Proteomic analysis of PMF-PT and PMF-BR spheroids. The Venn's diagram illustrates the overlapping and uniquely expressed proteins of the spheroids (E). Functional enrichment analysis of the uniquely expressed proteins in terms of the pathways found in PMF-PT and PMF-BR spheroids (F). Abbreviations: PMF-PT, PMF parental cell; PMF-BR, butyrate-resistant PMF cell.

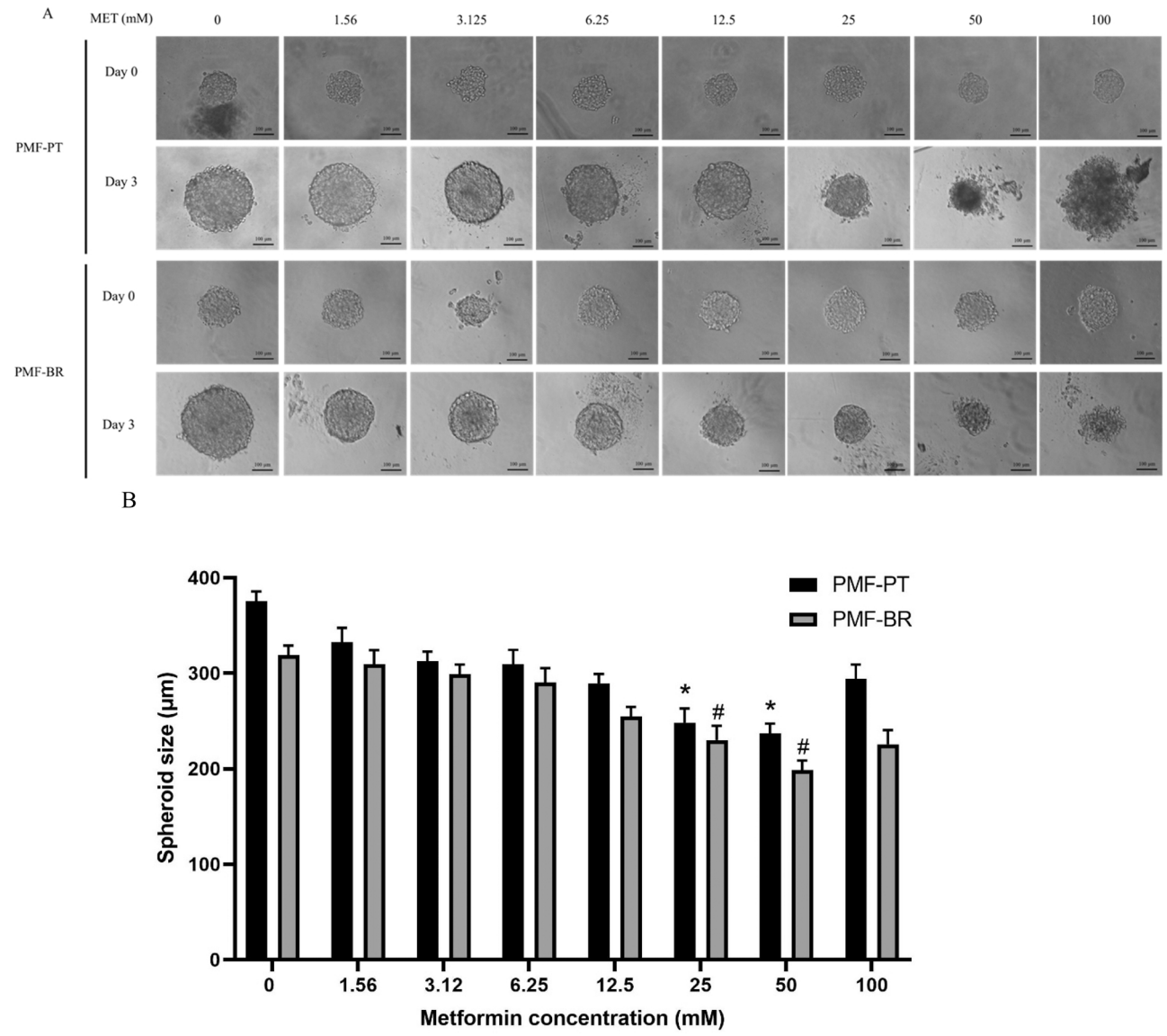

Fig. 3. Effect of MET on the size of PMF-PT and PMF-BR spheroids. The spheroids were incubated with various concentrations of MET for 72 h. Spheroids were imaged by inverted microscopy (10x magnification) (A). The bar graphs show the size of the spheroids. Scale bar= 100 μm. Significance: * p-value < 0.05 compared with PMF-PT control; MET 0 mM, # p-value < 0.05 compared with PMF-BR control; MET 0 mM. Abbreviations: PMF-PT, parental cell; PMF-BR, butyrate-resistant cell.

3.3. Molecular mechanism of MET in PMF-PT and PMF-BR spheroids

The primary mechanism associated with the activity of MET is the activation of the AMPK pathway and inhibition of the mTOR pathway. These two pathways are involved in the inhibition of proliferation and induction of apoptosis in many cancer cells. Therefore, the proteins related to them were examined. The expression of the proteins of interest in PMF-PT and PMF-BR spheroids following MET treatment was determined by Western blot analysis. Phospho-AMPK and p-Akt were significantly upregulated in the MET-treated group in both PT and BR spheroids. In addition, acetyl-CoA-carboxylase (ACC) was significantly reduced in the MET-treated group. We also found that p-mTOR exhibited lower expression in the MET-treated group; however, we found no significant difference in ratio of mTOR/p-mTOR expression. We also examined other molecules in the mTOR pathway. The expression of Raptor and Rictor were not different. The binding molecule of mTOR, Raptor, and Rictor is GβL. We found a significant decrease in GβL expression following MET treatment. Finally, c-Raf showed a significant decrease in MET-treated BR spheroids (Fig. 7). Altogether, these results suggested that MET could inhibit the cell viability of both PMF-PT and PMF-BR spheroids by activating the AMPK and Akt pathways and caspase activity and inhibiting the ACC and mTOR pathways.

4. Discussion

BR cells have been considered on the one of cancer-related chemoresistant and leading to treatment failure [8]. In this study, we induced the PMF-k014 cells with butyrate at the maximum concentration of 3.2 mM, whereas previous studies have used a lower butyrate concentration of 1.6 mM in CRC cell lines, including HCT-116, SW480, and HT29 cells, to induce as BR cells [8,26]. Unlike previous studies, we used PMF-k014 derived from metastatic colon adenocarcinoma, which is less responsive to anticancer drugs [27]. Moreover, previous studies have investigated several anticancer drugs tested in the 2D cell culture model, which is not adequately successful in clinical practice, whereas in vivo-like models such as the 3D culture are currently attracting significant attention. The present study is the first report to establish a butyrate-resistant PMF spheroid and its parental cell with a

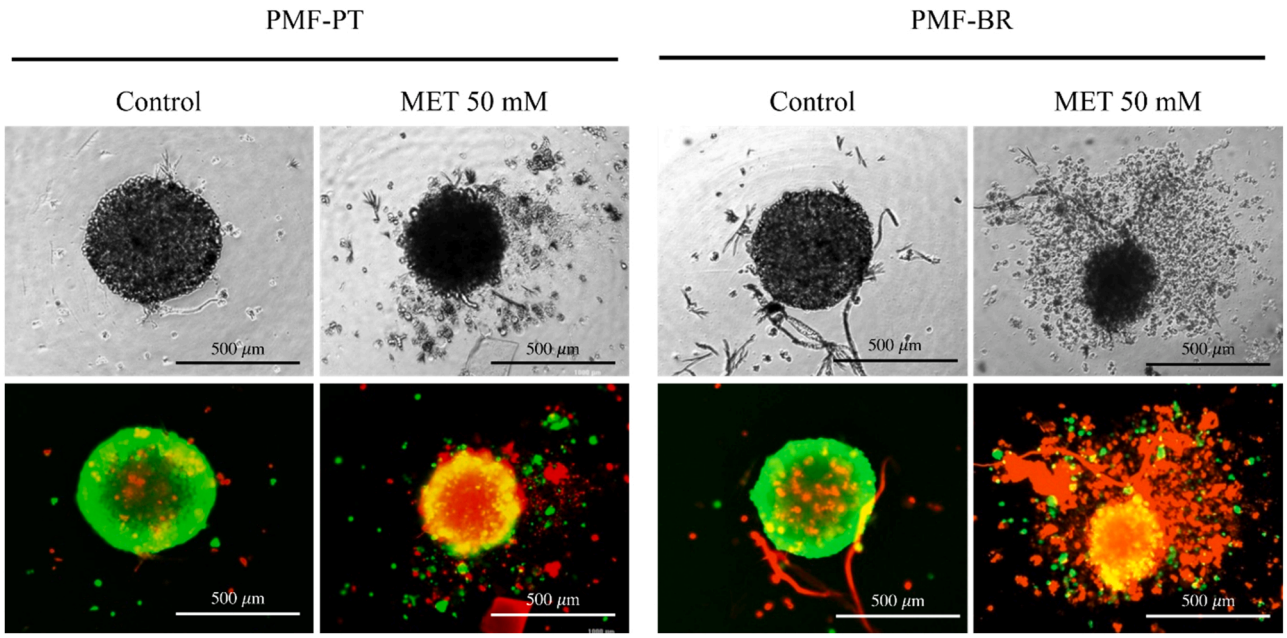

Fig. 4. Cytotoxic effect of MET on PMF-PT and PMF-BR spheroids. After being treated with MET at 50 mM for 72 h, the live/dead staining (live = green and dead = red) of the spheroids was imaged with a LionheartFX live cell imager (10x magnification). Scale bar = 500 μm. Abbreviations: PMF-PT, parental cell; PMF-BR, butyrate-resistant cell; MET 50 mM, MET treatment at 50 mM.

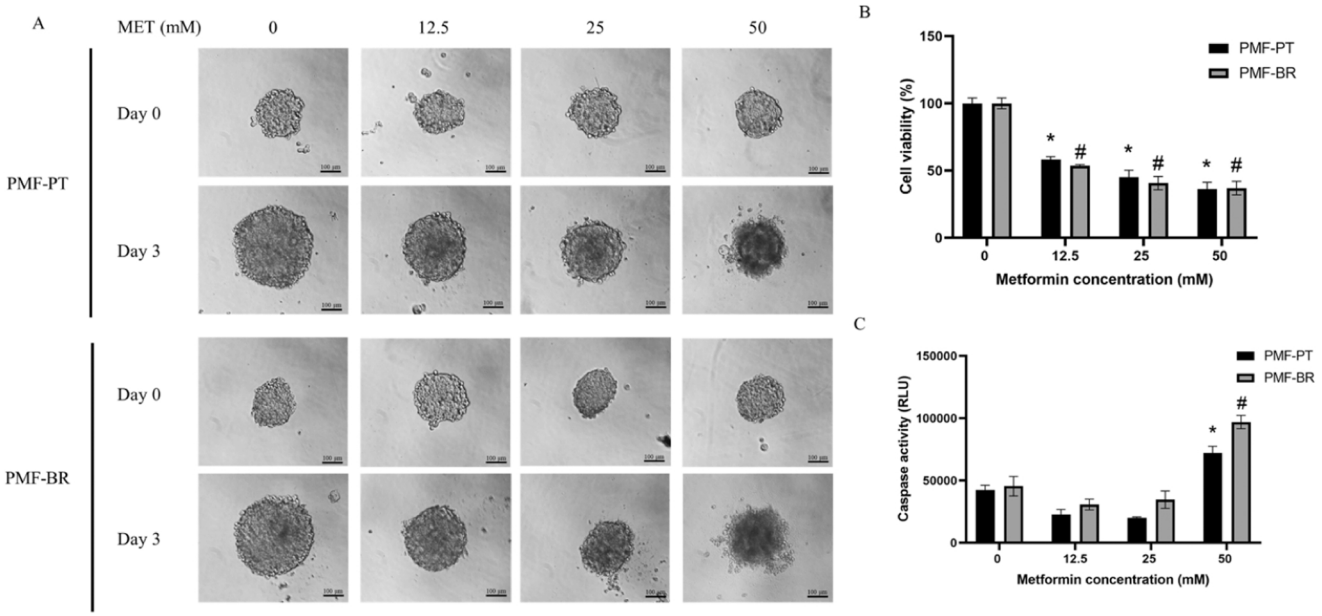

Fig. 5. MET-induced apoptosis in PMF-PT and PMF-BR spheroids. The morphology of the spheroids treated with and without MET at 0, 12.5, 25, and 50 mM for 72 h was visualized using an inverted microscope (10x magnification) (A). Scale bar = 100 μm. The ApoLive-Glo assay was used to detect cell viability (B) and caspase-3/7 activity (C). Statistical analysis was performed using the Student's *t*-test. Significance: * p-value < 0.05 compared with PMF-PT control; MET 0 mM, # p-value < 0.05 compared with PMF-BR control; MET 0 mM. Abbreviations: PMF-PT, parental cell; PMF-BR, butyrate-resistant cell.

round-shaped structure, compact morphology, and smooth surface, which is consistent with published results on CRC BCS-TC2. BR2 spheroids [28]. Numerous studies reported that 3D tumor spheroids including CRC, have enriched with CSC-like phenotype [29,30]. For example, the key stemness markers such as CD44 protein and *SOX2*, *OCT4*, *KLF4* genes were significantly higher expression in CRC HT-29 and Caco-2 spheroids than their 2D monolayers. This is in line with our study that both PMF-PT and PMF-BR spheroids showed the presence of CD44 on the membrane of cells in the spheroids. Moreover, *SOX2* and *OCT4* genes were also significantly high expression in PMF-PT and PMF-BR spheroids compared to their 2D monolayers.

Previous studies have also demonstrated that BR cells present a highly malignant phenotype, which includes traits such as survival in glucose depletion, inhibition of apoptosis, and resistance to anticancer drugs [6,7,31]; similarly, our findings demonstrated that PMF-BR spheroids were also cross-resistant to 5-FU. Several mechanisms are involved in the resistance to butyrate, including alteration of the drug target and, drug inactivation and efflux expression. To investigate the underlying mechanism in BR spheroids, we evaluated the expression of butyrate-related genes, including butyrate receptors, *GPR109A*,

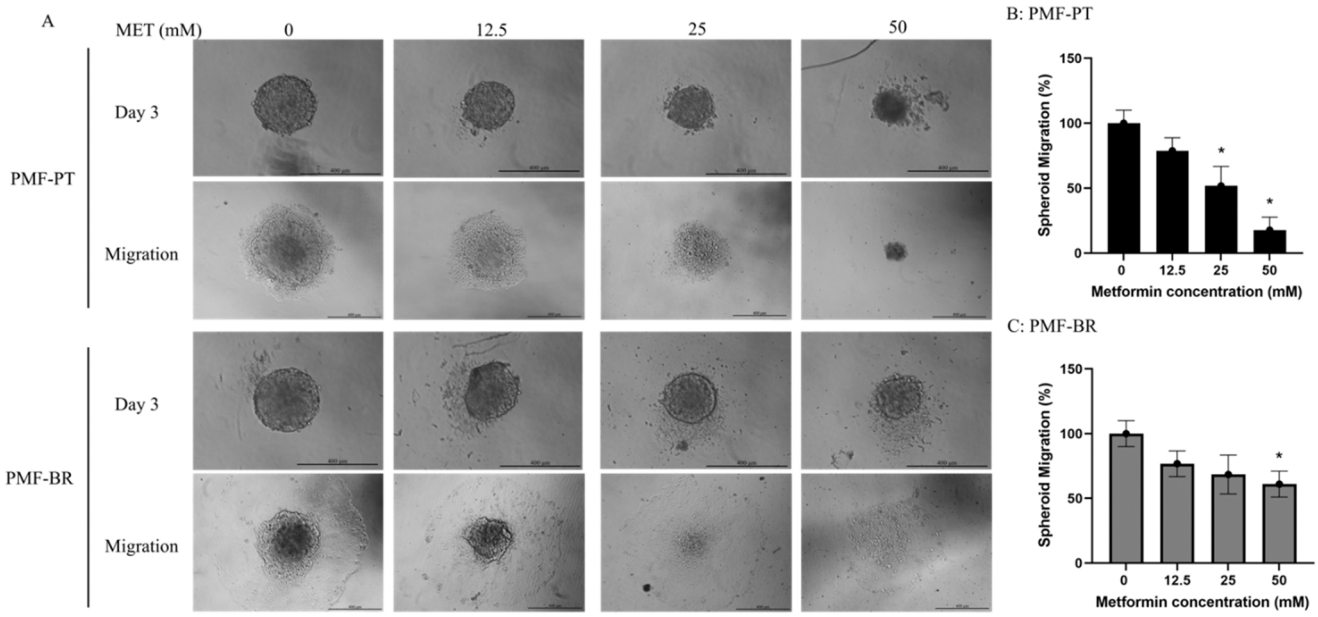

Fig. 6. Effect of MET on the cell migration of PMF-PT and PMF-BR spheroids. After the two spheroid cell types were treated with 0, 12.5, 25, and 50 mM of MET for 72 h, they were transferred to a flat-bottom plate and were further incubated for 72 h; their representative images were visualized using an inverted microscopy (10x magnification) (A). The bar graphs show the average percentage of the migration of PMF-PT (B) and PMF-BR (C) spheroids compared with the control value obtained from three independent experiments + SD (n = 3). Scale bar = 400 μm. Statistical analysis was performed using the Student's *t*-test. Significance: * *p*-value < 0.05 compared with the control; MET 0 mM. Abbreviations: PMF-PT, PT, parental cell; PMF-BR, BR, butyrate-resistant cell; MET, metformin treatment.

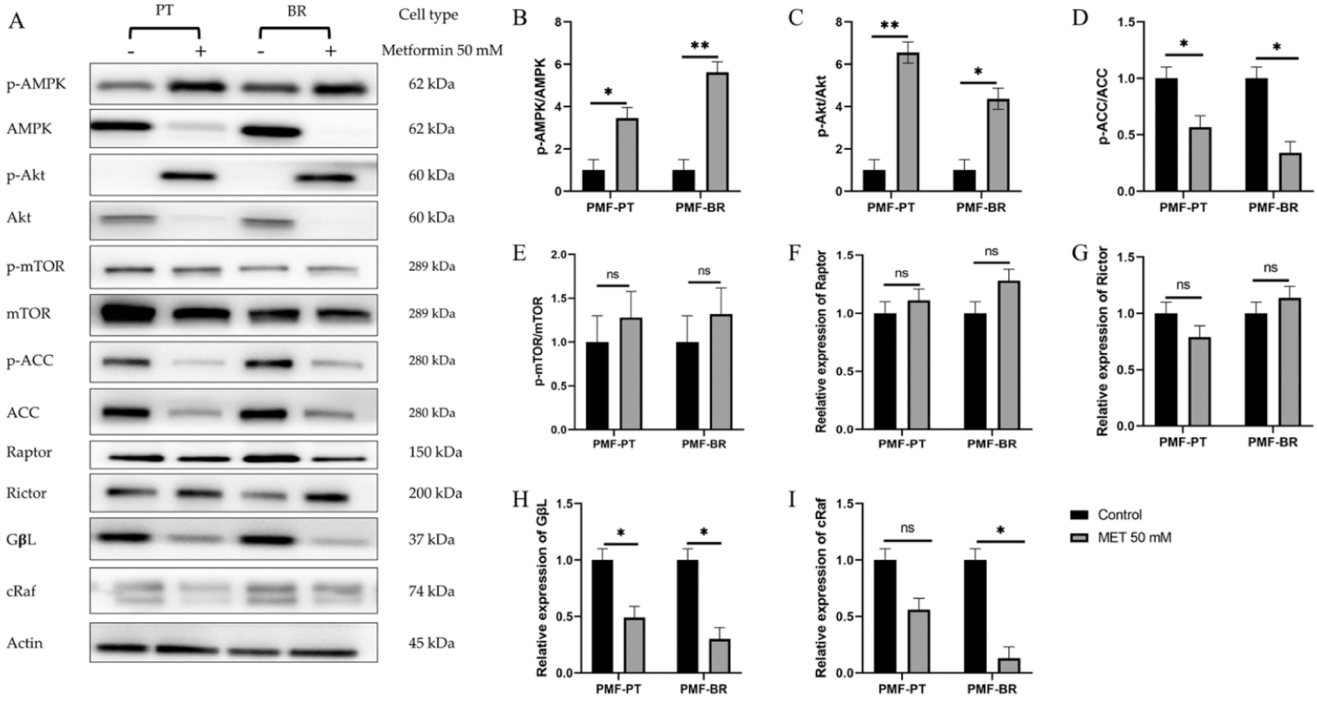

Fig. 7. Effect of MET on the AMPK/ACC/mTOR pathway and its binding proteins. Both PMF-PT and PMF-BR spheroids were treated with and without MET (50 mM) for 72 h. After incubation, the spheroids were collected and lysed by RIPA buffer. The total proteins were loaded on SDS-PAGE, and those of interest were examined by Western blot analysis. Actin was used as internal control (A). The quantitative proteins of interest, including p-AMPK/AMPK (B), p-Akt/Akt (C), p-ACC/ACC (D), p-mTOR/mTOR (E), Raptor (F), Rictor (G), GβL (H), and c-Raf (I), were normalized to actin band intensity. Data are shown as the mean ± SD of triplicate experiments. Statistical analysis was performed using Student's *t*-test. Significance: * *p*-value < 0.05 compared with the control; MET 0 mM. ** *p*-value < 0.01 compared with the control; MET 0 mM. Abbreviations: PMF-PT, PT, parental cell; PMF-BR, BR, butyrate-resistant cell; ns, non-significant; MET 50 mM, metformin treatment 50 mM.

GPR109B and *GPR-41*, and butyrate transporter, *SLC5A8*. PMF-BR spheroids showed an upregulation of *GPR109A*, *GPR109B*, and *GPR-41*. In a previous study, the expression of butyrate-related genes was upregulated in butyrate resistant mice (compared to germ-free mice) [32]. We further investigated the drug efflux gene expression. We found the expression of *ABC-C1*, *ABC-C2*, *ABC-C3*, *ABC-C5* and

ABC-G2 was upregulated in PMF-BR spheroids, whereas that of *ABC-A5* was upregulated in PMF-PT spheroids. Our finding is in line with the previous reports that have shown the upregulation of *ABC-C1* and *ABC-G2* in Hep2–5-FU-resistant cells [33]. These two ABC transporters are considered chemoresistance driven genes and play a role in the acquisition of chemoresistance. This finding would be the reason that PMF-BR spheroids were cross-resistant to 5-FU. Additionally, *ABC-C1*, *ABC-C3*, *ABC-C5* and *ABC-F2* are found in paclitaxel-resistant cells. Furthermore, doxorubicin resistance in breast cancer cells is induced by the overexpression of *ABC-C1* and *ABC-F2* [34,35]. In addition, cells expressing *ABC-A5* and *ABC-F2* are demonstrated to show stem cell features [36]. Moreover, we characterized the protein patterns between PT and BR spheroids. The proteins related to metabolic pathway and signal reception and transduction were found in PMF-BR greater than PMF-PT spheroids. For example, the proteins related to metabolic pathway in PMF-BR spheroids composed of proteins involved in glycolysis, gluconeogenesis, fructose, galactose, and pyruvate metabolism which are consistent with the previous research that showed upregulation of proteins in glycolysis/gluconeogenesis related to the higher rate of metabolism in rapid growing tumor cells [37]. While the proteins involved in glycolysis and TCA cycle were found lesser quantities in PMF-PT spheroids. Our finding indicated that many proteins related to metabolism process found in BR cells may help the cells to grow and survive in butyrate exposure condition. However, the molecular mechanism of butyrate resistance related to a cross-resistance of anti-cancer drugs should be addressed in further study. Moreover, the proteins related to apoptosis and stress response, DNA replication and repair, transcriptional and posttranscription process, and cell cycle control and proliferation were uniquely expressed in PMF-BR cells. The upregulation of the stress/apoptosis-related gene in particular proteins plays a role in the elimination of cytotoxic agents during chemotherapy for colon cancer [31].

Previous studies have attempted to overcome BR cells by targeting the AMPK pathway [9], which is a key pathway to balance the energy of cells and maintain homeostasis in various types of cancers [38]. The acquisition of butyrate resistance is associated with chemotherapeutic drug resistance, as mentioned above. The proposed mechanism of butyrate resistance included an increased p-Akt leading to decreased p-AMPK and p-ACC, resulting in the suppression of fatty-acid synthesis and apoptosis resistance [9]. To circumvent butyrate resistance in CRC cells, the activation of the AMPK pathway represents a promising strategy, as it would inhibit cell proliferation and coordinate metabolic reprogramming in drug-resistant cells [9]. MET, an anti-diabetic compound and AMPK activator drug, has been investigated as a cytotoxic drug in the tumoral cells of numerous cancer types, such as breast [39], cervical [38], and colorectal [40] cancers. MET primarily inhibits the mitochondrial respiratory chain complex I leading to AMPK activation [12,15]. MET is inexpensive and safe for diabetes patients, but its use is still controversial in cancer patients. However, retrospective studies of various cancer types showed the correlation between MET and lower cancer incidence, higher disease-free survival, and reduced cancer mortality [10,11,41,42]. Therefore, MET is a candidate for potential drug repurposing in cancer. Moreover, the combination of MET with conventional chemotherapy drugs showed a better anticancer effect compared to the use of chemotherapy alone [38,43,44]. MET also prevents doxorubicin resistance in breast cancer [16] and re-sensitizes the colorectal chemoresistant cancer cells [13]. Based on the above, MET may represent an effective treatment strategy for BR CRC cells. However, its effects on BR CRC cells using the 3D model have not been reported yet.

The present study demonstrated that the cytotoxic effect of MET on PMF-BR spheroids was dose-dependent. The spheroid morphology changed from a compact aggregation to a disaggregated state after MET treatment. We also detected an increase of caspase 3/7 activity following MET treatment, which resulted in apoptosis induction. The results are consistent with those reported in previous studies using the 2D culture model in breast, cervical, and CRC cells [38,39,45]. MET also inhibits PMF spheroid migration. However, it is necessary to further elucidate the anti-migration properties of MET in this cell type. Migration is a primary step for cell invasion and metastasis [46,47]. Previous studies have shown that MET inhibits cell migration in breast, pancreatic, and CRCs [13,46,47]. The molecular mechanism behind this inhibitory effect has also been previously elucidated. The inhibition of Akt/mTOR signaling was shown to reduce migration in squamous cell carcinoma [48], whereas the activation of AMPK/p53 with the inhibition of PI3K/Akt decreased migration in cervical cancer [49]. Further studies on the effect of MET on invasion should be conducted to the potential for use in cancer [50]. Cell invasion is one of the metastatic processes important for cancer cell distribution [51]. The inhibition of cell invasion by MET may be useful in cancer treatment.

The molecular mechanism of MET in PMF spheroids was determined by Western blot analysis. We found a significant upregulation of p-AMPK in the MET treatment group, and AMPK activation resulted in mTOR inhibition; however, we found no significant differences in the expression of mTOR-related molecules such as mTOR, p-mTOR, Raptor, and Rictor. Nevertheless, we observed a significant decrease in GβL, a binding factor of mTOR and its complex. The results suggested that AMPK activation reduces mTOR signaling by reducing the level of the binding molecules in PMF-BR spheroid cells. ACC, a key enzyme in fatty-acid synthesis, also significantly decreased, resulting in lipid synthesis inhibition and in the activation of fatty-acid oxidation. A previous study of head and neck cancer cells found that a higher ACC leads to an increased cell proliferation, whereas a lower level of this enzyme produces the opposite effect [52]. We observed upregulation of p-Akt in MET-treated spheroids. The overexpression of Akt and p-Akt occurs frequently in cancer cells. Because of its key role in cell survival, angiogenesis, and tumor formation, Akt is considered a hallmark of cancer [53]. Previous studies of human mesenchymal stem cells showed a significant activation of Akt, but not of AMPK, which resulted in cell survival following MET exposure [43]. In the present study, we also found a significant decrease of c-Raf in BR spheroids. This molecule plays an important role in apoptosis signaling and normally binds to the Bcl-2 protein, resulting in anti-apoptotic activity [54]. Decreased c-Raf levels result in the binding of Bcl-2 and BAD, leading to apoptosis.

Based on the overall results of this study, a proposed mechanism of MET action is presented in Fig. 8. It is concluded that the effect of MET is dependent on different regulatory pathways in the cells. MET activates AMPK which leads to mTOR pathway inhibition, a reduction in GβL expression, and cell cycle arrest. AMPK activation also leads to ACC inactivation, which results in a reduction of fatty-acid synthesis. Akt activation and c-Raf reduction result in the activation of caspase activity and apoptosis.

Altogether, our result demonstrated a potential cytotoxicity of MET on metastatic CRC cells at high concentration. However, it is necessary to evaluate the combination of MET and chemotherapeutic drugs to reduce the concentration of drugs and test in in vivo conditions before applying in clinical practice with low dose of MET.

5. Conclusions

In summary, MET shows potential therapeutic effects in PMF-BR spheroids through the activation of AMPK and Akt pathways and inhibition of the ACC and mTOR pathways leading to cell apoptosis. These findings suggest that MET is an effective treatment for drug-resistant CRC cells. Moreover, MET combined with chemotherapy should be further investigated as a strategy to treat CRC to improve the treatment and reduce the side effects of chemotherapy.

Funding

The research was supported by the Faculty of Medicine, Prince of Songkla University (REC6337942), the Research Center for Cancer

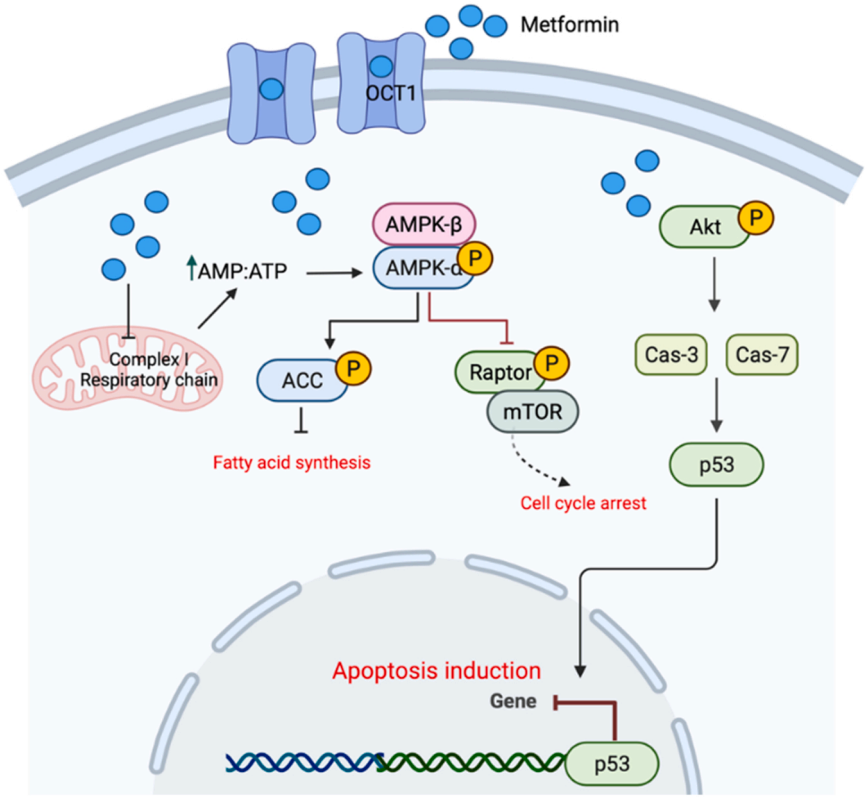

Fig. 8. Proposed mechanism of MET action through the AMPK/ACC/mTOR pathway in PMF-BR spheroids. Abbreviations: ACC, acetyl-CoA-carboxylase; Akt, RAC-alpha serine/threonine-protein kinase; AMPK, AMP-activated protein kinase; Cas, caspase; p53, mTOR, mammalian target of ra-pamycin; Protein 53; P, phosphorylation; OCT1, organic cation transporters 1; → means activation; ⊥ means inhibition.

Control in Thailand (MEDRC59036), and Graduate scholarship, Faculty of Medicine, Prince of Songkla University.

CRediT authorship contribution statement

Kesara Nittayaboon: Conceptualization, Methodology, Investigation, Data curation, Writing – original draft. **Kittinun Leetanaporn:** Software. **Surasak Sangkhathat:** Conceptualization. **Sittirak Roytrakul:** Software. **Raphatphorn Navakanitworakul:** Conceptualization, Writing – review & editing. All authors have read and agreed to the published version of the manuscript.

Conflicts of interest statement

The authors declare that there are no conflicts of interest.

Acknowledgments

The authors would like to thank Enago (www.enago.com) for the English language review.

Institutional review board statement

Not applicable.v

Appendix A. Supporting information

Supplementary data associated with this article can be found in the online version at doi:10.1016/j.biopha.2022.113214.

References

[1] H. Sung, J. Ferlay, R.L. Siegel, M. Laversanne, I. Soerjomataram, A. Jemal, F. Bray, Global cancer statistics 2020: GLOBOCAN estimates of incidence and mortality worldwide for 36 cancers in 185 countries, CA Cancer J. Clin. 71 (3) (2021) 209–249, https://doi.org/10.3322/caac.21660.

[2] V. Lohsiriwat, N. Chaisomboon, J. Pattana-Arun, Current colorectal cancer in Thailand, Ann. Coloproctol. 36 (2) (2020) 78–82. ⟨https://pubmed.ncbi.nlm.nih.gov/32054248⟩.

[3] K. Tiankanon, S. Aniwan, R. Rerknimitr, Current status of colorectal cancer and its public health burden in Thailand, Clin. Endosc. 54 (4) (2021) 499, https://doi.org/10.5946/ce.2020.245-IDEN.

[4] X. Wu, Y. Wu, L. He, L. Wu, X. Wang, Z. Liu, Effects of the intestinal microbial metabolite butyrate on the development of colorectal cancer, J. Cancer 9 (14) (2018) 2510–2517, https://doi.org/10.7150/jca.25324.

[5] M. Song, A.T. Chan, Diet, Gut microbiota, and colorectal cancer prevention: a review of potential mechanisms and promising targets for future research, Curr. Colorectal Cancer Rep. 13 (6) (2017) 429–439, https://doi.org/10.1007/s11888-017-0389-y.

[6] I.L. De Silanes, N. Olmo, J. Turnay, G. González De Buitrago, P. Pérez-Ramos, A. Guzmán-Aránguez, M. García-Díez, E. Lecona, M. Gorospe, M.A. Lizarbe, Acquisition of resistance to butyrate enhances survival after stress and induces malignancy of human colon carcinoma cells, Cancer Res. 64 (13) (2004) 4593–4600, https://doi.org/10.1158/0008-5472.CAN-04-0711.

[7] J.M. Mariadason, A. Velcich, A.J. Wilson, L.H. Augenlicht, P.R. Gibson, Resistance to butyrate-induced cell differentiation and apoptosis during spontaneous Caco-2 cell differentiation, Gastroenterology 120 (4) (2001) 889–899, https://doi.org/10.1053/gast.2001.22472.

[8] H.R. Kang, H.G. Choi, C.K. Jeon, S.J. Lim, S.H. Kim, Butyrate-mediated acquisition of chemoresistance by human colon cancer cells, Oncol. Rep. 36 (2) (2016) 1119–1126, https://doi.org/10.3892/or.2016.4838.

[9] H.Y. Yoo, S.Y. Park, S.-Y. Chang, S.H. Kim, Regulation of butyrate-induced resistance through AMPK signaling pathway in human colon cancer cells, Biomedicines Vol. 9 (2021), https://doi.org/10.3390/biomedicines9111604.

[10] J. Hanprasertpong, I. Jiamset, A. Geater, T. Peerawong, W. Hemman, S. Kornsilp, The Effect of metformin on oncological outcomes in patients with cervical cancer with type 2 diabetes mellitus, Int. J. Gynecol. Cancer 27 (1) (2017) 131–137, https://doi.org/10.1097/IGC.0000000000000855.

[11] Y.-L. Tang, L.-Y. Zhu, Y. Li, J. Yu, J. Wang, X.-X. Zeng, K.-X. Hu, J.-Y. Liu, J.-X. Xu, Metformin use is associated with reduced incidence and improved survival of endometrial cancer: a meta-analysis, Biomed. Res. Int. 2017 (2017) 1–9, https://doi.org/10.1155/2017/5905384.

[12] A. Fatehi Hassanabad, K.T. MacQueen, Molecular mechanisms underlining the role of metformin as a therapeutic agent in lung cancer, Cell Oncol. 44 (1) (2021) 1–18, https://doi.org/10.1007/s13402-020-00570-0.

[13] P. Nangia-Makker, Y. Yu, A. Vasudevan, L. Farhana, S.G. Rajendra, E. Levi, A.P. N. Majumdar, Metformin: a potential therapeutic agent for recurrent colon cancer, PLoS One 9 (1) (2014) 1–10, https://doi.org/10.1371/journal.pone.0084369.

[14] B. Viollet, B. Guigas, N. Sanz Garcia, J. Leclerc, M. Foretz, F. Andreelli, Cellular and molecular mechanisms of metformin: an overview, Clin. Sci. 122 (6) (2012) 253–270. ⟨https://www.ncbi.nlm.nih.gov/pubmed/22117616⟩.

[15] T.E. LaMoia, G.I. Shulman, Cellular and molecular mechanisms of metformin action, Endocr. Rev. 42 (1) (2021) 77–96, https://doi.org/10.1210/endrev/bnaa023.

[16] P.C. Marinello, C. Panis, T.N.X. Silva, R. Binato, E. Abdelhay, J.A. Rodrigues, A. L. Mencalha, N.M.D. Lopes, R.C. Luiz, R. Cecchini, A.L. Cecchini, Metformin prevention of doxorubicin resistance in MCF-7 and MDA-MB-231 involves oxidative stress generation and modulation of cell adaptation genes, Sci. Rep. 9 (1) (2019) 1–11, https://doi.org/10.1038/s41598-019-42357-w.

[17] M. Vinci, S. Gowan, F. Boxall, L. Patterson, M. Zimmermann, W. Court, C. Lomas, M. Mendiola, D. Hardisson, S.A. Eccles, Advances in establishment and analysis of three-dimensional tumor spheroid-based functional assays for target validation and drug evaluation, BMC Biol. (2012), https://doi.org/10.1186/1741-7007-10-29.

[18] S. Breslin, L. O'Driscoll, Three-dimensional cell culture: the missing link in drug discovery, Drug Discov. Today 18 (5–6) (2013) 240–249, https://doi.org/10.1016/j.drudis.2012.10.003.

[19] S. Lee, J. Hwa, H. Ki, J. Seok, B. Kim, J. Lee, J. Yun, G. Suk, M. Inoue, G. Choi, Colorectal cancer-derived tumor spheroids retain the characteristics of original tumors, Cancer Lett. (2015), https://doi.org/10.1016/j.canlet.2015.06.024.

[20] J. Koch, D. Mönch, A. Maaß, C. Gromoll, T. Hehr, T. Leibold, H.J. Schlitt, M.-H. Dahlke, P. Renner, Three dimensional cultivation increases chemo- and radioresistance of colorectal cancer cell lines, PLoS One 16 (1) (2021), e0244513. ⟨https://europepmc.org/articles/PMC7781370⟩.

[21] Y. Imamura, T. Mukohara, Y. Shimono, Y. Funakoshi, N. Chayahara, M. Toyoda, N. Kiyota, S. Takao, S. Kono, T. Nakatsura, H. Minami, Comparison of 2D- and 3D-culture models as drug-testing platforms in breast cancer, Oncol. Rep. 33 (4) (2015) 1837–1843, https://doi.org/10.3892/or.2015.3767.

[22] H. Karlsson, M. Fryknäs, R. Larsson, P. Nygren, Loss of cancer drug activity in colon cancer HCT-116 cells during spheroid formation in a new 3-D spheroid cell culture system, Exp. Cell Res. 318 (13) (2012) 1577–1585. ⟨https://www.sciencedirect.com/science/article/pii/S0014482712001620⟩.

[23] K. Okazaki, Y. Nakayama, K. Shibao, K. Hirata, T. Sako, N. Nagata, Y. Kuroda, H. Itoh, Establishment of a human colon cancer cell line (PMF-ko14) displaying highly metastatic activity, Int. J. Oncol. 17 (1) (2000) 39–45, https://doi.org/10.3892/ijo.17.1.39.

[24] S. Hirano, Western Blot Analysis. Nanotoxicity, Springer, 2012, pp. 87–97, https://doi.org/10.1007/978-1-62703-002-1_6.

[25] M. Vinci, C. Box, M. Zimmermann, S.A. Eccles, Tumor Spheroid-based Migration Assays for Evaluation of Therapeutic Agents. Target identification and validation in drug discovery, Springer, 2013, pp. 253–266, https://doi.org/10.1007/978-1-62703-311-4_16.

[26] H.Y. Yoo, S.Y. Park, S.-Y. Chang, S.H. Kim, Regulation of butyrate-induced resistance through AMPK signaling pathway in human colon cancer cells, Biomedicines 9 (11) (2021). ⟨https://www.mdpi.com/2227-9059/9/11/1604⟩.

[27] Y. Okada, T. Kimura, T. Nakagawa, K. Okamoto, A. Fukuya, T. Goji, S. Fujimoto, M. Sogabe, H. Miyamoto, N. Muguruma, EGFR downregulation after anti-EGFR therapy predicts the antitumor effect in colorectal cancer, Mol. Cancer Res. 15 (10) (2017) 1445–1454, https://doi.org/10.1158/1541-7786.MCR-16-0383.

[28] N. Olmo, J. Turnay, P. Perez-Ramos, E. Lecona, J.I. Barrasa, I.L. de Silanes, M. A. Lizarbe, In vitro models for the study of the effect of butyrate on human colon adenocarcinoma cells, Toxicol. Vitr. 21 (2) (2007) 262–270, https://doi.org/10.1016/j.tiv.2006.09.011.

[29] F.M. Robertson, M.A. Ogasawara, Z. Ye, K. Chu, R. Pickei, B.G. Debeb, W. A. Woodward, W.N. Hittelman, M. Cristofanilli, S.H. Barsky, Imaging and analysis of 3D tumor spheroids enriched for a cancer stem cell phenotype, J. Biomol. Screen 15 (7) (2010) 820–829, https://doi.org/10.1177/1087057110376541.

[30] E. Gheytanchi, M. Naseri, F. Karimi-Busheri, F. Atyabi, E.S. Mirsharif, M. Bozorgmehr, R. Ghods, Z. Madjd, Morphological and molecular characteristics of spheroid formation in HT-29 and Caco-2 colorectal cancer cell lines, Cancer Cell Int. 21 (1) (2021) 1–16, https://doi.org/10.1186/s12935-021-01898-9.

[31] N. Olmo, J. Turnay, E. Lecona, M. García-Díez, B. Llorente, A. Santiago-Gómez, M. A. Lizarbe, Acquisition of resistance to butyrate induces resistance to luminal components and other types of stress in human colon adenocarcinoma cells, Toxicol. Vitr. 21 (2) (2007) 254–261, https://doi.org/10.1016/j.tiv.2006.09.010.

[32] G.A. Cresci, M. Thangaraju, J.D. Mellinger, K. Liu, V. Ganapathy, Colonic gene expression in conventional and germ-free mice with a focus on the butyrate receptor GPR109A and the butyrate transporter SLC5A8, J. Gastrointest. Surg. 14 (3) (2010) 449–461, https://doi.org/10.1007/s11605-009-1045-x.

[33] M.B. Duz, O.F. Karatas, Expression profile of stem cell markers and ABC transporters in 5-fluorouracil resistant Hep-2 cells, Mol. Biol. Rep. 47 (7) (2020) 5431–5438, https://doi.org/10.1007/s11033-020-05633-x.

[34] J.P. Gillet, T. Efferth, D. Daniel Steinbach, J. Hamels, F. De Longueville, V. Bertholet, J. Remacle, Microarray-based detection of multidrug resistance in human tumor cells by expression profiling of ATP-binding cassette transporter genes, Cancer Res. 64 (2004) 8987–8993, https://doi.org/10.1158/0008-5472.CAN-04-1978.

[35] C.F. Thorn, C. Oshiro, S. Marsh, T. Hernandez-Boussard, H. McLeod, T.E. Klein, R. B. Altman, Doxorubicin pathways, Pharm. Genom. 21 (7) (2011) 440–446.

[36] M.B. Duz, O.F. Karatas, Differential expression of ABCB1, ABCG2, and KLF4 as putative indicators for paclitaxel resistance in human epithelial type 2 cells, Mol. Biol. Rep. 48 (2) (2021) 1393–1400.

[37] M.N. Song, P.G. Moon, J.E. Lee, M. Na, W. Kang, Y.S. Chae, J.Y. Park, H. Park, M. C. Baek, Proteomic analysis of breast cancer tissues to identify biomarker candidates by gel-assisted digestion and label-free quantification methods using LC-MS/MS, Arch. Pharm. Res. 35 (10) (2012) 1839–1847, https://doi.org/10.1097/FPC.0b013e32833ffb56.

[38] H.T. Kwan, D.W. Chan, P.C.H. Cai, C.S.L. Mak, M.M.H. Yung, T.H.Y. Leung, O.G. W. Wong, A.N.Y. Cheung, H.Y.S. Ngan, AMPK activators suppress cervical cancer cell growth through inhibition of DVL3 mediated Wnt/β-catenin signaling activity, PLoS One 8 (1) (2013) 1–10, https://doi.org/10.1371/journal.pone.0053597.

[39] I.N. Alimova, B. Liu, Z. Fan, S.M. Edgerton, T. Dillon, S.E. Lind, A.D. Thor, Metformin inhibits breast cancer cell growth, colony formation and induces cell cycle arrest in vitro, Cell Cycle 8 (6) (2009) 909–915, https://doi.org/10.4161/cc.8.6.7933.

[40] S.J. Koh, J.M. Kim, I.K. Kim, S.H. Ko, J.S. Kim, Anti-inflammatory mechanism of metformin and its effects in intestinal inflammation and colitis-associated colon cancer, J. Gastroenterol. Hepatol. 29 (3) (2014) 502–510, https://doi.org/10.1111/jgh.12435.

[41] A. DeCensi, M. Puntoni, P. Goodwin, M. Cazzaniga, A. Gennari, B. Bonanni, S. Gandini, Metformin and cancer risk in diabetic patients: a systematic review and meta-analysis, Cancer Prev. Res. 3 (11) (2010) 1451–1461, https://doi.org/10.1158/1940-6207.CAPR-10-0157.

[42] S. Gandini, M. Puntoni, B.M. Heckman-Stoddard, B.K. Dunn, L. Ford, A. DeCensi, E. Szabo, Metformin and cancer risk and mortality: a systematic review and meta-analysis taking into account biases and confounders, Cancer Prev. Res. 7 (9) (2014) 867–885, https://doi.org/10.1158/1940-6207.CAPR-13-0424.

[43] R. Würth, A. Pattarozzi, M. Gatti, A. Bajetto, A. Corsaro, A. Parodi, R. Sirito, M. Massollo, C. Marini, G. Zona, D. Fenoglio, G. Sambuceti, G. Filaci, A. Daga, F. Barbieri, T. Florio, Metformin selectively affects human glioblastoma tumor-initiating cell viability, Cell Cycle 12 (1) (2013) 145–156, https://doi.org/10.4161/cc.23050.

[44] H.A. Hirsch, D. Iliopoulos, K. Struhl, Metformin inhibits the inflammatory response associated with cellular transformation and cancer stem cell growth, Proc. Natl. Acad. Sci. 110 (3) (2013) 972–977. ⟨https://www.pnas.org/content/110/3/972⟩.

[45] J. He, K. Wang, N. Zheng, Y. Qiu, G. Xie, M. Su, W. Jia, H. Li, Metformin suppressed the proliferation of LoVo cells and induced a time-dependent metabolic and transcriptional alteration, Sci. Rep. 5 (October) (2015) 1–16, https://doi.org/10.1038/srep17423.

[46] B. Bao, Z. Wang, S. Ali, A. Ahmad, A.S. Azmi, S.H. Sarkar, S. Banerjee, D. Kong, Y. Li, S. Thakur, F.H. Sarkar, Metformin inhibits cell proliferation, migration and invasion by attenuating CSC function mediated by deregulating miRNAs in pancreatic cancer cells, Cancer Prev. Res. 5 (3) (2012) 355–364, https://doi.org/10.1158/1940-6207.CAPR-11-0299.

[47] C. Schexnayder, K. Broussard, D. Onuaguluchi, A. Poché, M. Ismail, L. McAtee, S. Llopis, A. Keizerweerd, H. McFerrin, C. Williams, Metformin inhibits migration and invasion by suppressing ROS production and COX2 expression in MDA-MB-231 breast cancer cells, Int. J. Mol. Sci. 19 (11) (2018) 3692, https://doi.org/10.3390/ijms19113692.

[48] C. Harsha, K. Banik, H.L. Ang, S. Girisa, R. Vikkurthi, D. Parama, V. Rana, B. Shabnam, E. Khatoon, A.P. Kumar, A.B. Kunnumakkara, Targeting AKT/mTOR in oral cancer: mechanisms and advances in clinical trials, Int. J. Mol. Sci. Vol. 21 (2020), https://doi.org/10.3390/ijms21093285.

[49] Y.-H. Chen, P.-H. Wang, P.-N. Chen, S.-F. Yang, Y.-H. Hsiao, Molecular and cellular mechanisms of metformin in cervical cancer, Cancers Vol. 13 (2021), https://doi.org/10.3390/cancers13112545.

[50] F. Weiss, D. Lauffenburger, P. Friedl, Towards targeting of shared mechanisms of cancer metastasis and therapy resistance, Nat. Rev. Cancer 22 (3) (2022) 157–173, https://doi.org/10.1038/s41568-021-00427-0.

[51] N.H. Ha, F. Faraji, K.W. Hunter, Mechanisms of metastasis, Cancer Target Drug Deliv. Elus. Dream. 9781461478 (2013) 435–458.

[52] Li K., Chen L., Lin Z., Zhu J., Fang Y., Du J., Shen B., Wu K., Liu Y., 2020. Role of the AMPK/ACC Signaling Pathway in TRPP2-Mediated Head and Neck Cancer Cell Proliferation. Saponaro G., editor. Biomed Res Int. 2020;2020:4375075. https://doi.org/10.1155/2020/4375075.

[53] J.R. Testa, A. Bellacosa, AKT plays a central role in tumorigenesis, Proc. Natl. Acad. Sci. 98 (20) (2001) 10983–10985. ⟨https://pubmed.ncbi.nlm.nih.gov/11572954⟩.

[54] U.R. Rapp, U. Rennefahrt, J. Troppmair, Bcl-2 proteins: master switches at the intersection of death signaling and the survival control by Raf kinases, Biochim. Biophys. Acta - Mol. Cell Res. 1644 (2) (2004) 149–158. ⟨https://www.sciencedirect.com/science/article/pii/S0167488903001812⟩.